2009 IEEE 11th International Conference on Rehabilitation Robotics
Kyoto International Conference Center, Japan, June 23-26, 2009

Design and control of two planar cable-driven robots for upper-limb neurorehabilitation

Giulio Rosati, Damiano Zanotto, Riccardo Secoli, Aldo Rossi

Abstract— **Post-stroke robot-aided neurorehabilitation is an emerging research field, aiming to improve the intensity and the effectiveness of post-stroke rehabilitation protocols by using robotic technology and virtual reality. One classification that has been proposed for therapy robots is between exoskeletons and end-effector based machines. The latter are those devices whose interaction with the patient's arm takes place at the end-effector level.**

This paper presents the design of two novel end-effector based robots for upper-limb rehabilitation, named Sophia-4 and Sophia-3. Although the devices are based on a common concept (the cable-drive actuation over a planar workspace), the latter differs from the former by the number of employed cables (4 and 3, respectively), and, by several design solutions, such as the introduction of a moving pulley-block to enhance workspace and a tilting table to better target the patient's shoulder. Both mechanical and control system design are addressed and a comparison of performances is presented.

I. Introduction

Stroke is a leading cause of movement disability in the developed countries. Every year in the U.S. and Europe there are 200 to 300 new stroke cases per 100.000, the 30% of whom survive with important motor deficits [1], [2]. Due to population aging, this trend is going to grow further in the next decades [2]. Motor training after stroke is thus becoming a primary societal goal, based on the increasing evidence that the motor system is plastic following stroke and can be influenced by motor training [3].

Many mechatronic systems have been developed in the last two decades to help post-stroke recovery of the upper and the lower limbs. The rationale for using robotic devices in rehabilitation is that there is strong evidence that highly repetitive movement training, with active engagement by the participant, promotes cortical re-organization and can result in improved recovery after stroke [4], [5]. Robotic devices can be employed to help automate repetitive training in a controlled fashion, and to increase treatment compliance by introducing incentives to the patient, such as games or performance-related scores [6].

Two recent reviews on the first Randomized Controlled Trials (RCTs) of upper-limb robot-assisted rehabilitation outlined that clinical results are still far from being fully satisfactory [6], [7]. In fact, even though motor recovery is usually greater in therapy groups, only few studies showed some positive results at the functional level, the summary effect size of the studies being very close to zero. These results suggest that the therapy devices, exercises and protocols developed so far still need to be improved and optimized, with the aim of helping the patients in regaining their abilities in the Activities of Daily Living (ADLs), to favor their reintegration into social and domestic life.

All authors are with the Faculty of Engineering, Department of Innovation in Mechanics and Management (DIMEG), University of Padua, via Venezia 1, 35131 Padova, Italy giulio.rosati@unipd.it

According to a common classification [8], two kind of robotic devices can be identified: the exoskeleton-like machines and the end-effector based machines. Some recent examples of robotic systems developed along the first line include [9], [10], [11]. These kind of robotic devices allow a complete control of the human arm trajectories, both in joint space and in task space. However, exoskeletons require a complex mechanical design to guarantee a precise alignment of robot and human joints, which is always difficult to achieve in a reasonably wide range of motion. Moreover, due to the need of producing high torques at joint level, these robotic systems often employ gear reducers. As a result, backdrivability can be compromised, and complex control strategies must be implemented to obtain an acceptable level of robot compliance. Compliance can be considered a highly desirable feature for therapy robotics, as it preserves the causal relationship between patient effort and resulting arm movement, even when robotic assistance is provided [12].

End-effector based machines, also referred to as operational-type devices, are those systems in which human-robot interaction takes place at a single interface (the end-effector). They are easier to design, cheaper and safer if compared to exoskeletons. However, they do not allow control on single human joints and cannot even measure human joint displacements, velocities, torques, etc. Among the operational-type devices designed for upper limb motor rehabilitation, planar robots are notable for their simple architecture. The MIT/Manus represents the most famous example of this class: the shoulder and elbow module, a 2-degrees-of-freedom (dof) SCARA-like robot developed in 1991, has recently been improved with a spatial extension [13] and with new wrist and hand modules to obtain the stimulation of the whole arm [14], [15]. Cartesian-type devices have also been designed: the Memos [16] and, more recently, the CBM-Motus, an isotropic belt-driven planar device [17].

This paper focuses on the design of two novel cable-driven devices currently being developed at the Rehabrobotics Lab at DIMEG, University of Padua, Italy. The use of cable actuation in neurorehabilitation robots has already been proposed [18], in particular our research group developed two cable-suspended systems for upper-limb rehabilitation, the NeReBot and the MariBot [19]. The former undergone a first clinical trial with stroke patients in the acute and sub-acute

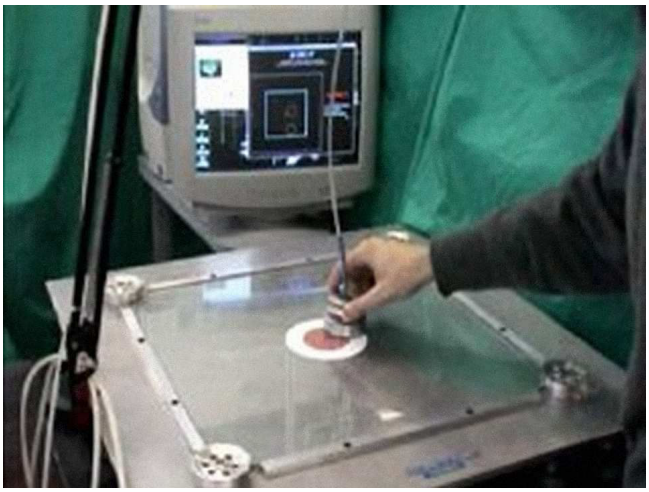

Fig. 1. Overview of the FeRiBa3 cable-driven haptic display [21], [22]. In this picture, an operator is interacting with a virtual planar environment.

phase, with encouraging results on both motor and functional evaluation scales [20]. The novel devices presented here, the Sophia-3 and Sophia-4 (String Operated Planar Haptic Interface for Arm-rehabilitation-n, where n is the number of cables), came up as an evolution of a planar haptic display, named FeRiBa3, developed some years ago [21], [22]. In this device, four driven cables are exploited to produce two force components and one moment on the end-effector handled by the operator (see figure 1). Each cable is attached to the end-effector at one end, and wound around a driven pulley at the opposite end. The pulley blocks are placed at the corners of a square. If compared to other planar solutions, cable-driven design leads to similar or even better performances, especially in terms of inertial properties (mass perceived at the end-effector and isotropicity) and force capabilities [23]. In this paper, the design and control of the Sophia devices are presented.

II. Design

Figure 2 shows a concept drawing of the Sophia devices. In both systems the patient, while sitting on a wheelchair, holds a handlebar-grip that can be moved over a flat horizontal surface. The driven cables are all attached to a single point of the end-effector, so the device is capable of exerting only horizontal pure forces on the patient's hand. The handlebar-grip itself is mounted on the base of the end-effector by means of a ball bearing, in such a way that no moment can be transmitted to the patient's hand along the vertical axis. The resulting force produced by the cables on the end-effector is computed in real-time by a high-level controller, while the end-effector position and the cable tensions are calculated by a low-level controller. The data on the status of the current exercise, together with a real-time visual feedback, are displayed on a PC monitor in front of the patient.

A. Layout of the pulley-blocks

Two major aspects have been considered in the early design of the devices: workspace shape and force capabilities. Due to unilateral actuation (i.e., cables can only pull), the number of cables must be greater than the number of required forces: this is usually referred to as *actuation redundancy*. Under the pseudo-static hypothesis, the structure matrix $\mathbf{A}$ relates the vector of cable tensions $\mathbf{f}$ to the operational force $\mathbf{F}$ through the linear *force-closure equation* [24]:

$$\mathbf{A}\mathbf{f} = \mathbf{F} \tag{1}$$

For a given design, the matrix $\mathbf{A}$ depends only on the position of the end-effector. In addition, if n denotes the number of dofs and m the number of cables, matrix $\mathbf{A} \in M_{n\times m}$. The statics workspace is defined as the set of positions wherein any operational force $\mathbf{F}$ can be exerted on the end-effector with all positive cables tensions (i.e., $\mathbf{f} \geq \mathbf{0}$) [25]. In the case of planar cable-driven point-mass devices, the statics workspace coincides with the convex hull of the cable attachment points [26].

In principle, once the number of cables has been decided, the position of the pulley-blocks can be adjusted to match the patient's reachable workspace. However, since cable tensions are necessarily constrained (i.e. $f_{\min} \leq \mathbf{f} \leq f_{\max}$), force performances are also dependent on end-effector position

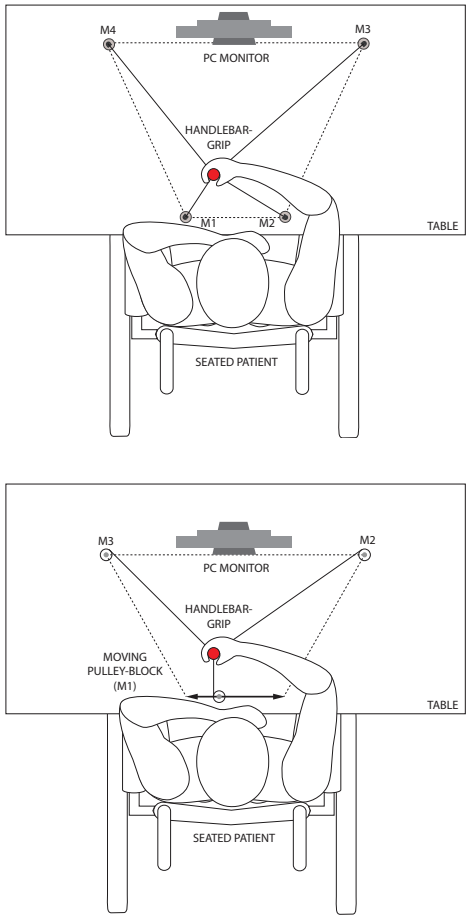

Fig. 2. Schematic top-view of the Sophia-4 (top) and the Sophia-3 (bottom). The first device has four cables attached to fixed pulley-blocks (M1, M2, M3, M4), whereas the second robot employs three pulleys which are directly connected to the EE through the cables, and the lower pulley is movable.

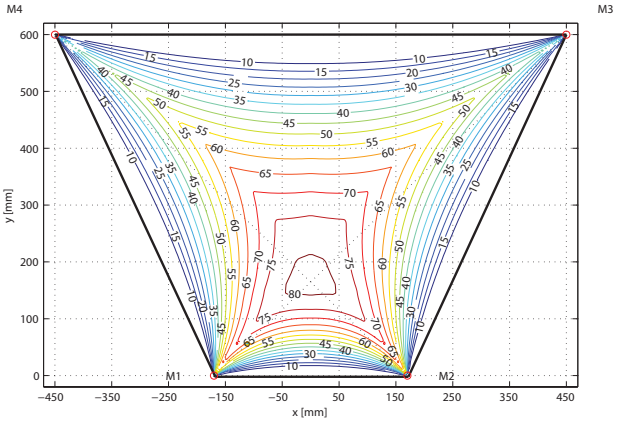

Fig. 3. Contour plot of the force index i_F [N] for Sophia-4, calculated with $f_{\max} = 87N$ and $f_{\min} = 5N$. The maximum isotropic force is greater than 60N inside most of the workspace.

within the statics workspace, so the useful workspace may be significantly smaller than the theoretical one. For planar point-mass devices, the magnitude of the maximum isotropic force i_F can be used to quantify the force capabilities all through the workspace. This parameter expresses the magnitude of the maximum force that can be exerted in any direction of the workspace for a given position of the end-effector [24]. This value is particularly significant in this application field, since the force produced by the device during the execution of a rehabilitation exercise is not predictable, as it depends not only on the implemented exercise but also and mainly on patient's behavior. A detailed description on force performance indexes for cable-driven robots may be found in [24].

Figure 3 shows the contour plot of i_F and the final layout of pulley-blocks for Sophia-4, with the following constraints on the tensions in cables: $f_{\min} = 5N$, $f_{\max} = 87N$. The trapezoidal layout allow the patient to lean his/her elbows outside the lower pulley-blocks, thus avoiding arm-cable interference. The length of the lower base has been determined based on the average shoulder distance of adult males [27].

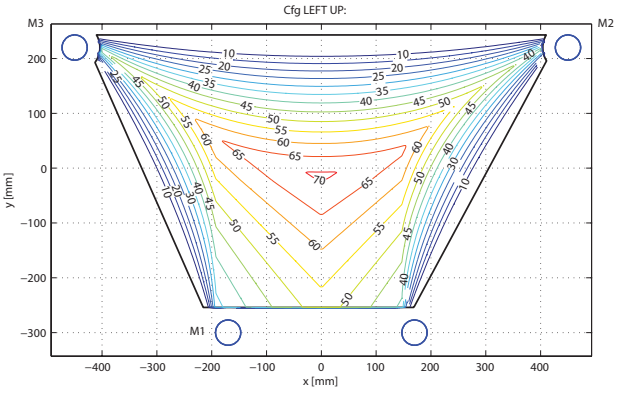

Fig. 4. Contour plot of i_F [N] for Sophia-3. The reduced number of actuators yields smaller i_F with respect to Sophia-4. Nonetheless, a static force greater than $50N$ is obtained inside most of the workspace.

Comparable force capabilities can be maintained even with 2 upper pulley-blocks and one lower pulley-block, provided that the latter can be moved according to the position of the end-effector [28]. The design of Sophia-3 takes advantage of this concept: the lower pulley-blocks have been substituted with a moving pulley-block, whose range of motion equals the length of the lower base in the previous design. The height of the trapezium has been reduced in order to move the most favorable region of the workspace closer to the patient. Figure 4 shows the resulting i_F diagram, obtained by moving the lower pulley block to track the x position of the end-effector. In this way, the lower cable is kept orthogonal to the guide, unless the end of travel is reached.

By comparing figure 3 and figure 4, it can be noticed that the useful region of the workspace (i.e., $i_F \geq 50N$), even though slightly smaller in the new device, is suitable in both cases. The second scheme is better in that the lower portion of the workspace is much better in terms of force capabilities with respect to the Sophia-4. In fact, the boundary effect caused by cables alignment is totally eliminated near the linear guide. Moreover, the reduced number of cables allows for more free motions of the patient's arm in the same portion of the workspace, with no possibility of cable-arm interference.

B. Sophia-4

A commercial office table constitutes the mechanical structure of Sophia-4. An aluminum handbar-grip can be moved on the wooden surface, sliding on low-friction PTFE discs. Four nylon cables, $\Phi = 1mm$, are used to exert forces at the end-effector, each having one end fixed to a point on the axis of the grip, and the other directly keyed to a direct-drive pulley. Pulley-blocks which can spin around a vertical axis are used to pass cables underneath the table surface, where the DC motors are mounted (rated continuous torque $1.4Nm$). Optical encoders ($4000ppr$) are used for forward kinematics, while the tension in each cable is controlled by commanding the winding current.

C. Sophia-3: new design with a tilting table-top

The Sophia-3, whose first prototype is currently being assembled, shares most of the design solutions adopted in the previous device, with some modifications. A new structure made of modular aluminum elements supports the table, which can rotate around a fixed longitudinal axis, located under the table, next to the patient's legs. Table orientation can be varied in the range $0 - 60°$ to change the kinematics of the exercises: the patient can be exercised in moving the hand over a rising surface. With the aim of reducing friction, a PTFE cover is to be mounted over the wooden surface, and pulley blocks have been eliminated. As a consequence, pulleys and motors have been moved upward, next to the plane of motion. More powerful AC brushless motors (rated to $2.15Nm$ of continuous torque) actuate the upper pulleys, while a gearmotor (rated to $2.38Nm$ of output torque) is used for the moving pulley-block. The linear motion of the lower pulley block is achieved through a miniature ball screw. All

components are mounted on the bottom surface of the table, or partially embedded in it. All dimensions have been chosen to comply with the UFAS requirements [29]. To facilitate the displacements of the device, wheels have been installed on the bottom of each table leg.

III. Control System

A similar control architecture has been designed for the two devices. The main embedded real-time controller (PC/104 stack) runs both the high-level control and the low-level control. While the former manages the type of assistance to be given, the latter is responsible for low-level routines, such as kinematics, force distribution algorithms and surveillance routines. The Human-Machine Interface (HMI) runs on a separate standard PC, allowing the therapist to set the type of exercise and its parameters, and providing the patient with visual and acoustic feedback. Each exercise is composed by a sequence of point-to-point reaching tasks. The target point of each portion of the exercise is calculated by the HMI and transmitted to the controller, that is programmed to implement single reaching tasks.

A. Low level control

The low level control is responsible for several tasks, among which the computation of the vector of cable tensions $\mathbf{f}$ that yields the desired assistive force $\mathbf{F}$ calculated by the high level control. According to the linear system (1), for a given $\mathbf{F}$, if $m > n$ and the end-effector lays inside the workspace, an infinite set of *allowable solutions* (i.e. those solutions satisfying: $f_{\min} \leq \mathbf{f} \leq f_{\max}$) exists, so a force distribution algorithm must be implemented to obtain a suitable solution.

1) Numerical algorithm: a common technique consists in writing equation (1) as a constrained optimization problem:

$$\min_{\mathbf{f}\in R^m} \left(\tfrac{1}{2}\mathbf{f}^T\mathbf{I}_m\mathbf{f}\right), \quad \text{subject} \quad \text{to}: \begin{cases} \mathbf{A}\mathbf{f} = \mathbf{F} \\ f_{\min} \leq \mathbf{f} \leq f_{\max} \end{cases} \tag{2}$$

The Kuhn-Tucker method can then be applied to determine the optimal solution. This is a general algorithm that fits any number of cables m. Simulations and experimental tests showed smoother tension paths when the upper bound is removed from 2, and a suitable *force scaling* algorithm is applied to the optimal solution.

2) Geometrical algorithm: the numerical method proved to be robust, even though computationally expensive. Thus, in order to reduce computational timing, two geometric algorithms have been implemented, for planar point-mass systems with $m = 3$ or $m = 4$. When $n = 2$ and $m = 3$ (Sophia-3), the system is completely restrained. For any system belonging to this class, a theorem presented in a previous work [21] states the existence and uniqueness of the minimum-norm allowable solution $\hat{\mathbf{f}}$, as long as the end-effector lays inside the workspace. Also, an explicit expression for the solution has been derived in [21]:

$$\begin{cases} \hat{\mathbf{f}} = \tilde{\mathbf{f}}_\mathbf{i} + \beta\mathbf{h} \\ \beta = \max\limits_{t=1,2,3} \left(\frac{f_{\min} - \tilde{\mathbf{f}}_\mathbf{i}(t)}{\mathbf{h}(t)}\right) \end{cases} \tag{3}$$

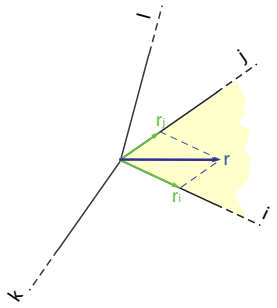

Fig. 5. Decomposition of $\mathbf{r}$ into its components along the nearest cables.

where $\tilde{\mathbf{f}}_\mathbf{i}$ is a solution of equation (1) having the i-th component arbitrarily set to zero (i.e. $\tilde{\mathbf{f}}_\mathbf{i}(i) = 0$), and $\mathbf{h}$ is the strictly-positive kernel vector of $\boldsymbol{A}$.

When a degree of redundancy is added (i.e., $n = 2$ and $m = 4$, the case of Sophia-4), the derivation of an explicit expression for the minimum-norm solution is not straightforward. To get an approximated method, we first normalize equation (1) by $f_{\min}$. In this way, any allowable tension vector can be rewritten as the sum of a minimum required contribution and a non-negative add-on: $\mathbf{f}/f_{\min} = \begin{bmatrix} 1 & 1 & 1 & 1 \end{bmatrix}^T + \boldsymbol{\tau}$. The former may be mapped to the operational space through the matrix $\boldsymbol{A}$, and its contribute subtracted from $\mathbf{F}/f_{\min}$. This leads to a new simplified formulation of equation 1:

$$\boldsymbol{A}\boldsymbol{\tau} = \mathbf{r} \tag{4}$$

where $\mathbf{r} = \left(\mathbf{F}/f_{\min} - \mathbf{A}\begin{bmatrix} 1 & 1 & 1 & 1 \end{bmatrix}^T\right)$ is the contribution to the operational force due to $\boldsymbol{\tau} \geq 0$. The simplest way to obtain an allowable $\boldsymbol{\tau}$ consist in decomposing $\mathbf{r}$ into two component vectors, along the directions of the nearest pair of cables containing $\mathbf{r}$ (figure 5).

Even though this approach is likely to yield the minimum-norm solution, discontinuities are to be expected in the tension paths every time $\mathbf{r}$ gets across one cable, and the angle between the new *active pair* of cables is significantly different from that of the previous pair. Sudden changes in the tensions of the cables have a detrimental effect on the stability of the haptic interface, so that this method is quite inadequate for our purposes. Starting from equation (4), a new geometric algorithm has been developed, leading to an explicit expression for the actual minimum-norm solution. Since three-cable equilibrium may occur during changes of the active pair, this method does not show discontinuities, and also shortened computation times to almost $1/10$ of those of the numerical algorithm. A detailed description of the new algorithm will be presented in a future work.

Since the numerical and the geometrical approaches do not account for the upper bound $f_{\max}$, a method must be applied to *scale* the cable tensions vector $\mathbf{f}$ if one of its components exceeds $f_{\max}$. Given the linearity of system (1), by scaling vector $\mathbf{f}$ we will get an actual operational force with the same direction as $\mathbf{F}$ and a magnitude reduced by the scaling factor. The scaling factor can be chosen so the tension of

the most stressed cable is kept equal to $f_{\max}$. Without this correction, the saturation of one or more actuators may lead to significant differences between the required force $\mathbf{F}$ and the actual force.

For example, let us consider a flat elastic virtual wall with $k = 3N/mm$, located at $y_W = 150mm$ (figure 6). As the end-effector approaches the virtual wall, moving on a vertical straight trajectory, positive cable tensions are computed to yield a null operational force $\mathbf{F} = 0$ (figure 7). As soon as the end-effector enters the wall, an elastic reaction force is generated along y. For a certain value of y_{EE}, the required force causes the most loaded cable to reach the upper constraint $f_{\max}$. A further increment in the magnitude of $\mathbf{F}$ would lead to the saturation of the same cable, and the actual vector of cable tensions would therefore differ in one component from the computed one, which satisfies equation (1). This, in general, will result in an exerted force that differs from the required one in both magnitude and direction.

Figure 7 clearly shows that, after saturation of cable 1, the exerted force acquires an unwanted x component at the expense of the needed y component. The situation gets even worse as the second cable saturates. Figure 8 shows the effects of force scaling in the previous example: once cable 1 has reached $f_{\max}$, its value is kept constant by properly scaling the whole vector of cable tensions. This, in turn, will only reduce the magnitude of the required operational force, without changing its orientation. Such a behavior is clearly more suitable for the a haptic device, providing the user with a more natural force feedback.

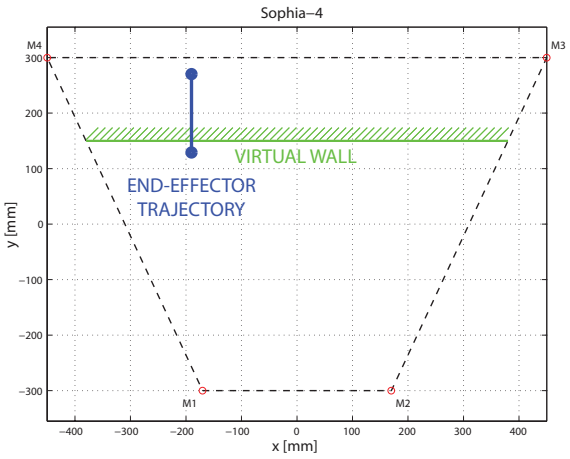

Fig. 6. Test-case straight trajectory against a $3N/mm$ stiff virtual wall.

B. High level control

Once the low level controller is implemented, the planar devices can be used to employ any kind of high-level control. A first option is impedance control. In this case, the point-to-point reaching movements that compose the exercise are assisted by creating a tunnel-like force field placed around the nominal trajectory. Null forces are felt by the patient as long as he/she moves the end-effector inside the tunnel, whereas assistive forces are provided by elastic virtual walls

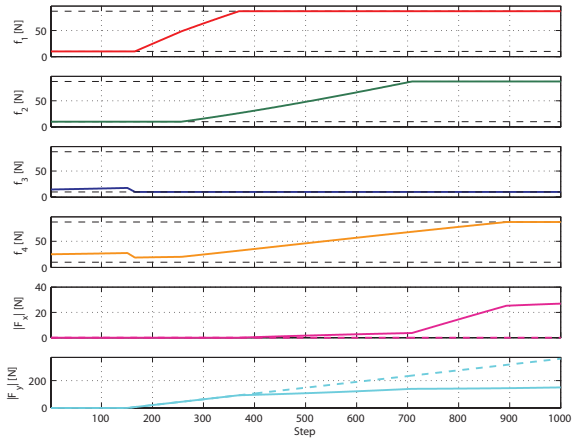

Fig. 7. Cable tensions and end-effector forces along the path shown in figure 6, without tension scaling. As one or more cable tensions saturate, an unwanted x force is produced and the end-effector force changes direction.

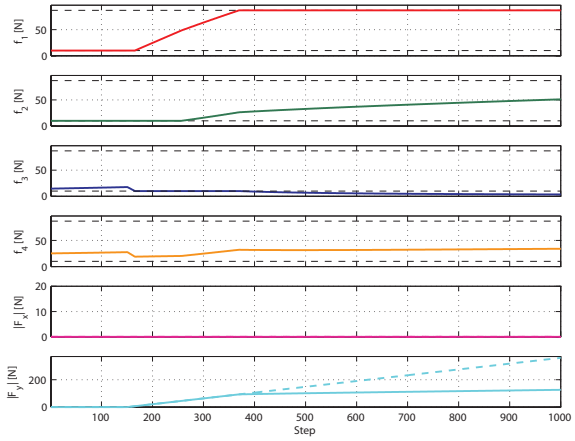

Fig. 8. Cable tensions and end-effector forces along the path shown in figure 6, with tension scaling. The direction of the end-effector force is always correct, even when one or more cable tensions saturate.

as soon as the end-effector comes out of the tunnel. In addition, the control system can help the patient to complete the movement, if a certain lack of progress is noted.

A second control algorithm implemented in the Sophia devices is the adaptive controller with a forgetting term first introduced by Wolbrecht et al. [10]. The control law representing the original model-based adaptive control is:

$$\mathbf{F_r} = \mathbf{Y}\hat{\mathbf{a}} - \mathbf{K}_P\,(\mathbf{x} - \mathbf{x_d}) - \mathbf{K}_P\,(\dot{\mathbf{x}} - \dot{\mathbf{x}}_\mathbf{d}) \qquad (5)$$

where $\mathbf{x}$ and $\mathbf{x_d}$ are the current and desired (planned) location of patient's hand, $\mathbf{K}_P$ and $\mathbf{K}_D$ are the proportional and derivative gain matrices, and $\mathbf{Y}$ is the regressor matrix, containing vectors of Gaussian radial basis functions. Vector of parameter estimates $\hat{\mathbf{a}}$ represents the magnitudes of the radial basis functions, whose value is determined by adding to the standard sliding surface update law an exponential decay. The latter acts as a *forgetting term*, preventing the controller from 'taking over' the patient [1]. This behavior is

[1]For a detailed description of the algorithm, please refer to [10]

similar to that of a therapist, who tries to 'learn' a model of patient's behavior and then to assist him/her providing the minimum amount of assistance 'as needed'.

If the matrix $\mathbf{Y}$ is a function of position only [10], the control system can learn very easily position-dependent force fields. However, during repetitive planar reaching exercises, the planned trajectory may pass through the same position several times requiring different assistive forces, which in turn will cause variations of the model. Hence, the adaptive gain must be large enough to rapidly change the model, and this in turn decreases robot compliance. To avoid this limitation, two improvements have been proposed in [12], that allow to increase robot compliance while still accurately achieving target movements. The idea is either to employ movement specific models (i.e., multiple parameter estimates vectors) or to use time-based Gaussian basis functions. These approaches are alternative to that of introducing velocity and acceleration based models, whose computational cost would be hard to afford on a real-time controller.

IV. Conclusion

This paper presented two different designs for a planar robotic therapy device, conceived for post-stroke rehabilitation of the upper limbs. The most convenient 4-cable and 3-cable layouts have been derived first, based on the optimization of force performances. Then, the mechanical structures of both prototypes were introduced, followed by a description of control system architecture. Both prototypes derive their design from a previously developed cable-driven haptic display, that implemented impedance control. New design solutions have been introduced, such as a moving pulley-block to enhance workspace, a tilting table to better target the patient's shoulder, and a point-mass end-effector to eliminate torque exertion on the patient's wrist. At the same time, the control architecture has been improved, both at low-level (by introducing fast geometrical algorithms for the computation of cable tensions) and at high level (by implementing a model-based adaptive controller).

References

[1] W Rosamond, K Flegal, et al. Heart disease and stroke statistics-2007 update: A report from the american heart association statistics committee and stroke statistics subcommittee. *Circulation*, 115:69–171, 2007.

[2] G. Boysena T. Truelsena, M. Ekmanb. Cost of stroke in europe. *European Journal of Neurology*, 12:78–84, 2005.

[3] R J Nudo. Postinfarct cortical plasticity and behavioral recovery. *Stroke*, 38(2):840–845, 2007.

[4] C. Butefisch, H. Humelsheim, P. Denzler, and K.H. Mauritz. Repetitive training of isolated movements improves the outcome of motor rehabilitation of the centrally paretic hand. *J Neurol Sci.*, 130(1):56–68, 1995.

[5] J. Liepert, H. Bauder, H. R. Wolfgang, W. H. Miltnerand E. Taub, and C. Weiller. Treatment-induced cortical reorganization after stroke in humans. *Stroke*, 31:1210–6, 2000.

[6] G Kwakkel, B J Kollen, and H I Krebs. Effects of robot-assisted therapy on upper limb recovery after stroke: A systematic review. *Neurorehabilitation and Neural Repair*, 22:111–121, 2007.

[7] J Mehrholz, T Platz T, J Kugler, and M Pohl. Electromechanical and robot-assisted arm training for improving arm function and activities of daily living after stroke (review). *Cochrane Database of Systematic Reviews*, 4, 2008.

[8] M Mihelj, T Nef, and R Riener. Armin ii - 7 dof rehabilitation robot: mechanics and kinematics. In *Proc. of the IEEE Int. Conf. on Robotics and Automation 2007*, pages 4120–4125, April 2007.

[9] T. Nef, M. Mihelj, G. Kiefer, C. Perndl, R. Muller, and R. Riener. Armin - exoskeleton for arm therapy in stroke patients. *Proc. of the IEEE 10th Int. Conf. on Rehabilitation Robotics ICORR2007*, pages 68–74, June 2007.

[10] Eric T Wolbrecht, Vicki Chan, David J Reinkensmeyer, and James E Bobrow. Optimizing compliant, model-based robotic assistance to promote neurorehabilitation. *IEEE Transactions on Neural Systems and Rehabilitation Engineering*, 16(3):286–297, 2008.

[11] A. Frisoli, L. Borelli, A. Montagner, et al. Arm rehabilitation with a robotic exoskeleleton in virtual reality. In *Proc. of the IEEE 10th Int. Conf. on Rehabilitation Robotics ICORR2007*, Noordwijk, The Netherlands, June 2007.

[12] G. Rosati, J. E. Bobrow, and D. J. Reinkensmeyer. Compliant control of post-stroke rehabilitation robots: using movement-specific models to improve controller performance. In *Proc. of the ASME International Mechanical Engineering Congress & Exposition IMECE 2008*, Boston, MA, USA, Oct 31 - Nov 6 2008.

[13] H I Krebs, M Ferraro, et al. Rehabilitation robotics: Pilot trial of a spatial extension for mit-manus. *J. Neuro Eng. Rehabil.*, 1:1–15, 2004.

[14] H I Krebs, B T Volpe, et al. Robot-aided neurorehabilitation: A robot for wrist rehabilitation. *IEEE Transactions on Neural Systems and Rehabilitation Engineering*, 15(3):327–335, 2007.

[15] L Masia, H I Krebs, P Cappa, and N Hogan. Design and characterization of hand module for whole-arm rehabilitation following stroke. *IEEE/ASME Transactions on Mechatronics*, 12(4):339–407, 2007.

[16] Roberto Colombo, Fabrizio Pisano, et al. Robotic techniques for upper limb evaluation and rehabilitation of stroke patients. *IEEE Transactions on Neural Systems and Rehabilitation Engineering*, 13(3):311–324, September 2005.

[17] L Zollo, D Accoto, F Torchiani, D Formica, and E Guglielmelli. Design of a planar robotic machine for neuro-rehabilitation. In *Proc. of the IEEE Int. Conf. on Robotics and Automation*, 2008.

[18] G. Rosati, P. Gallina, A. Rossi, and S. Masiero. Wire-based robots for upper-limb rehabilitation. *International Journal of Assistive Robotics and Mechatronics*, 7(2):3–10, 2006.

[19] G. Rosati, M. Andreolli, A. Biondi, and P. Gallina. Performance of cable suspended robots for upper limb rehabilitation. In *Proc. of the IEEE 10th Int. Conf. on Rehabilitation Robotics ICORR2007*, pages 385–392, Noordwijk, the Netherlands, June 13-15 2007.

[20] S. Masiero, A. Celia, G. Rosati, and M. Armani. Robotic-assisted rehabilitation of the upper limb after acute stroke. *Archives of Physical Medicine and Rehabilitation*, 88(2):142–149, 2007.

[21] P. Gallina and G. Rosati. Manipulability of a planar wire driven haptic device. *Mechanism and Machine Theory*, 37(2):215–228, 2002.

[22] P. Gallina, G. Rosati, and A. Rossi. 3-d.o.f. wire driven planar haptic interface. *J. of Intelligent and Robotic Systems*, 32(1):23–36, 2001.

[23] G. Rosati, R. Secoli, D. Zanotto, A. Rossi, and G. Boschetti. Planar robotic systems for upper-limb post-stroke rehabilitation. In *Proc. of the ASME International Mechanical Engineering Congress & Exposition IMECE 2008*, Boston, MA, USA, Oct 31 - Nov 6 2008.

[24] G. Rosati, D. Zanotto, and A. Rossi. Performance assessment of a 3d cable-driven haptic device. In *Proc. of the ASME International Mechanical Engineering Congress & Exposition IMECE 2008*, Boston, MA, USA, Oct 31 - Nov 6 2008.

[25] P Gallina, A Rossi, and R L Williams II. Planar cable-direct-driven robots, part ii: Dynamics and control. In *Proc. of the ASME Design Engineering Technical Conf.*, volume 2, pages 1241 – 1247, 2001.

[26] P. Lafourcade and M. Llibre. First steps toward a sketch-based design methodology for wire-driven manipulators. In *Proc. of the 2003 IEEE/ASME Int. Conf. on Advanced Intelligent Mechatronics (AIM)*, volume 1, pages 143–148 vol.1, 20-24 July 2003.

[27] Wilfred Taylor Dempster. Space requirements of the seated operator, geometrical, kinematic, and mechanical aspects of the body with special reference to the limbs. Technical report, Defense Technical Information Center, U.S., July 1955.

[28] G Rosati and D Zanotto. A novel perspective in the design of cable-driven systems. In *Proc. of the ASME International Mechanical Engineering Congress & Exposition IMECE 2008*, Boston, MA, USA, Oct 31 - Nov 6 2008.

[29] U.S. Architectural and Transportation Barriers Compliance Board, Federal Register, 49 FR 31528. *Uniform federal accessibility standards*, August 7 1984.